International Journal of Innovation and Scientific Research
ISSN 2336-0046 Vol. 82 No. 1 Dec. 2025, pp. 8-23

http://www.ijisr.issr-journals.org/

Contribution to the comparative study of DC-DC converter topologies for the regulation and control of electrical systems: The case of an electric vehicle

Batassou Guilzia Jeannot[1-3], Fouda Bella Regine[2], Koko Koko Joseph[1-2], and Ndjakomo Essiane Salomé[2-4]

[1]Laboratory of Computer and Automatic Engineering, UFD of Engineering Sciences (ENSET), University of Douala, Cameroon

[2]Higher Normal School of Technical Education ENSET of Ebolowa. University of Ebolowa, Cameroon

[3]National Advanced School of Public Works of Yaoundé (ENSTP). Yaoundé Cameroon, BP 510 Elig-Effa, Cameroon

[4]Higher Technical Training College of Douala. University of Douala. Douala, Cameroon

ABSTRACT: In recent years, the reliability and continuity of service of powertrains have become major challenges for electric vehicles to enter the mass market. Indeed, defects in powertrains lead to malfunctions in vehicles and reduce their performance compared to conventional vehicles. In this article, we focus on the DC/DC converter associated with the fuel cell in the powertrain. The latter must address the major issues facing fuel cell electric vehicle applications, namely: low mass and small volume, high energy efficiency, reduction of input current ripple, and reliability. This work then consisted of sizing and testing the fault-tolerant DC/DC converter structure selected for P to C vehicles. Algorithms for managing the degraded modes of this converter were developed and implemented experimentally. In this regard, the interaction between P to C and the DC/DC converter was studied. A theoretical simulation approach was used to carry out this work. This approach made it possible, under the most demanding conditions, to achieve very high efficiencies in steady state for both converters: 97.2% for the VS = 400V version and 95.5% for the VS = 200V version, powered respectively by input voltages of 400V and 200V. For input voltages in the lowest range, the efficiency is naturally lower. However, we are confident that this criterion ($\eta \geq 96\%$) will be met over the nominal voltage range (between 300 and 600V). This demonstrator has validated the real benefits of a two-stage structure for applications with high input voltage variation, with each stage achieving efficiency in excess of 98%.

KEYWORDS: electric vehicle, DC/DC converter, analytical method, electrical system control, fuel cell.

1 INTRODUCTION

Electric vehicles (EVs) are at the heart of the global energy transition, offering a cleaner and more efficient alternative to traditional internal combustion vehicles [1]. Central to this transition are highly efficient and reliable power management systems, including DC-DC (direct current to direct current) converters [2]. These converters play a crucial role in regulating and controlling electrical energy within electric vehicles, enabling the conversion of battery voltage to appropriate levels to power various vehicle components, such as motors, electronic systems, and auxiliary devices.

DC-DC converters must meet several critical requirements: high efficiency, compactness, robustness, and the ability to handle load and voltage variations. However, there are several DC-DC converter topologies [3], each with its own advantages and disadvantages in terms of performance, cost, and complexity [4]. The central issue of this comparative study is to determine which DC-DC converter topology is best suited for regulating and controlling electrical systems in an electric vehicle, taking into account the following criteria: energy efficiency, compactness and weight, heat management, robustness and reliability, cost, and ease of control.

This comparative study aims to: analyze the different DC-DC converter topologies and other advanced configurations such as resonant converters, evaluate the performance of each topology, and finally identify the trade-offs between the different topologies and determine which ones offer the best balance between performance criteria for application in electric vehicles.

Corresponding Author: Batassou Guilzia Jeannot

2 TOOLS AND ANALYSIS METHODS

2.1 TOOLS

Several simulation tools were used to analyze our system. Similarly, computer-aided design tools have become indispensable in various industrial sectors. These tools for predicting and analyzing system behavior reduce the costs and time required to study a new product by delaying the actual implementation of prototypes. The implementation of our system requires the use of certain necessary tools, namely software and mathematical tools. As part of our work, we will use MATLAB-Simulink for the modeling and simulation of our system.

2.2 METHODS

As part of this work, the choice of analytical method breaks down the system into simple elements, optimizes each element (analysis of failure, cause, consequence, and criticality), and aggregates the whole by simple aggregation, subject to verification of the proper interlocking of the optimized elements [5], [6]. For the comparative study of DC-DC converter topologies for the regulation and control of electrical systems in electric vehicles, the following working hypotheses will be explored to guide the research and analysis: Resonant DC-DC converters, such as LLC converters, offer higher energy efficiency than non-resonant topologies such as Buck, Boost, and Buck-Boost converters in electric vehicle applications [6]; Multi-level converters and integrated topologies offer higher power density and increased compactness compared to conventional topologies (Buck, Boost, Buck-Boost) in electric vehicle power management systems. DC-DC converters using wide bandgap semiconductors (SiC, GaN) offer superior robustness and reliability under extreme operating conditions compared to converters using silicon semiconductors; Resonant DC-DC converters generate fewer harmonics and offer better output wave quality than non-resonant converters [7], [8].

2.2.1 DESIGN METHODOLOGY FOR ISOLATED DC/DC CONVERTERS WITH PARALLEL RESONANCE FOR ELECTRIC VEHICLES

The electric vehicle powertrain studied uses a fuel cell as its energy source, whose role is to provide the average power required by the vehicle. It is connected to the DC bus via a unidirectional DC/DC converter. The vehicle is powered by a permanent magnet synchronous motor connected to a three-phase inverter, which is supplied with power by the DC bus. The powertrain of the electric vehicle under study is shown in Figure 1.

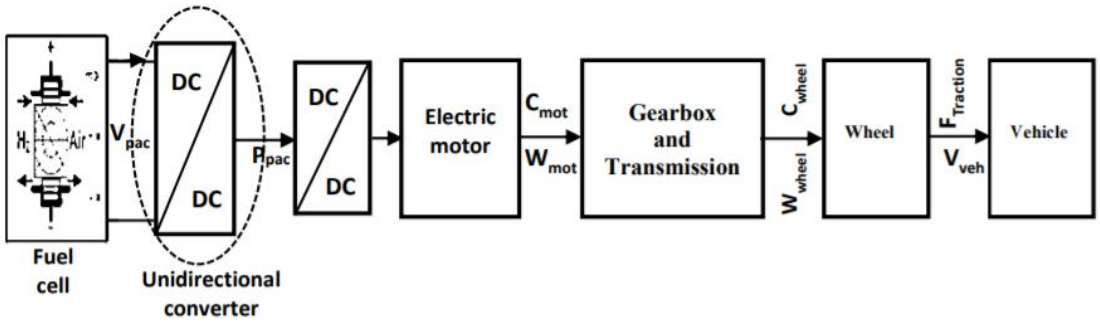

Fig. 1. Electric vehicle powertrain under study

2.2.2 LOAD MODELING

The behavior of a vehicle moving along its direction of travel is determined by all the forces acting on it in that direction. Figure 2 shows the forces acting on a vehicle on a slope.

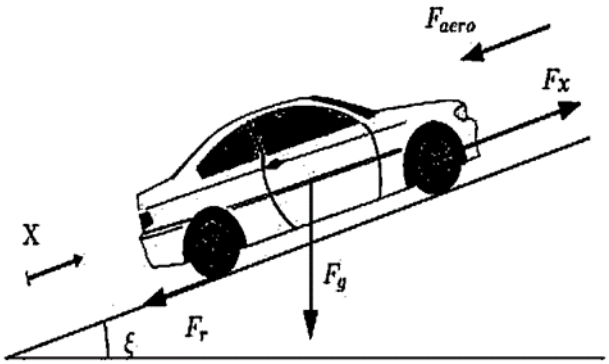

Fig. 2. Forces applied to the vehicle [9]

With:

- F_r: rolling resistance force, it acts on the tires and opposes the free movement of the vehicle. It is caused by the deformation of the tires on the road, which generates rolling resistance;

$$F_r = M.g.C_r \quad (1)$$

It depends on the vehicle mass M (kg), the acceleration due to gravity g (m/s-2), and the rolling resistance coefficient Cr [10].

- F_g: Gravity acts directly on the vehicle on slopes. It holds it back when going uphill and pushes it downhill. It depends on the slope angle ξ and the vehicle mass M. The expression for the force of gravity is given by equation (2):

$$F_g = M.g.\sin(\varepsilon) \quad (2)$$

- $F_{aéro}$: is the force of air resistance. It varies according to the speed of the vehicle and depends on nonlinear phenomena related to fluid mechanics. It is proportional to the density of air ρ (kg/m^3), the frontal area of the vehicle Sf (m^2), the drag coefficient Cx, and the vehicle speed V (m/s). It is given by equation (3) [11];

$$F_{aero} = \frac{\rho C_X S_f V^2}{2} \quad (3)$$

- F_x: Traction force refers to the force exerted at the periphery of the drive wheels in contact with the ground to create or maintain vehicle movement.

$$F_x = M\frac{dV(t)}{dt} + M.g.\sin(\vartheta) + \frac{\rho C_X S_f V^2}{2} + M.g.C_r \quad (4)$$

2.2.3 FUEL CELL MODELING

We are interested in modeling a single cell. The voltage of a PEM fuel cell drops as a function of the current delivered due to losses. These losses are due to irreversibilities and manifest themselves in three ways: activation losses, ohmic losses, and concentration losses [12], [13].

The expression for the voltage of a PEM fuel cell is shown in equation (5).

$$V_{cell} = E_{Nernst} - \Delta V_{act} - \Delta V_{ohm} - \Delta V_{conc} \quad (5)$$

$$\text{With} \begin{cases} E_{Nernst} = E_o + \frac{RT}{2F}\ln\left(\frac{P_{H_2}\sqrt{P}O_2}{P_{H_2O}}\right) \\ \Delta V_{act} = \frac{RT}{2\alpha F}\ln\left(\frac{i_{PAC}}{i_0}\right) \\ \Delta V_{ohm} = R_{PAC} i_{PAC} \\ \Delta V_{conc} = -\frac{RT}{2\alpha F}\ln\left(1 - \frac{i_{PAC}}{i_0}\right) \end{cases} \quad (6)$$

Where

E_{Nernst}: Represents the potential of Nernst;

ΔV_{act}: represents activation losses due to the initiation of chemical reactions at the anode and cathode;

α: represents the transport coefficient;

i_0 exchange current density;

$\Delta V_{ohm:}$ represents the ohmic losses due to the resistance of the electrodes and bipolar plates to the flow of electrons and electrolyte during the passage of protons;

R_{PAC}: the total resistance of the fuel cell;

$\Delta V_{conc:}$ represents the overvoltage of the concentration;

PH2, PO2, PH2O: are the pressures of hydrogen, oxygen, and water, respectively.;

T: is the cell temperature (Kelvin);

R: is the ideal gas constant (8.31441 J. mol^{-1}. K^{-1});

F: is Faraday's constant (96484.56 C.mol^{-1}).

The voltage equation for a PEM fuel cell can be represented by an equivalent electrical circuit shown in Figure (3). This circuit is a simplified model of the fuel cell.

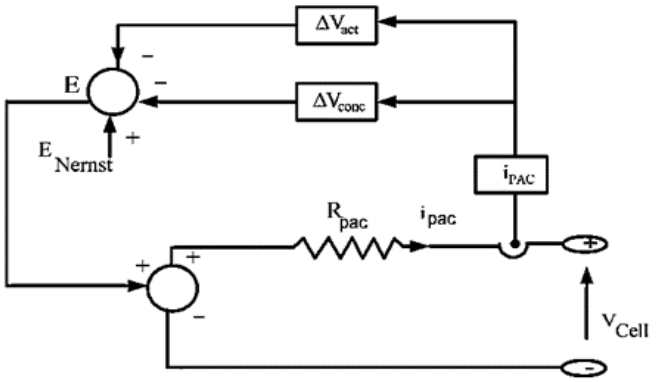

Fig. 3. Simplified electrical model of a fuel cell cell [14]

2.2.4 SIZING OF ISOLATED RESONANT DC/DC CONVERTERS

For each topology, we write its system of differential equations, whose state variables are the currents in the inductors and the voltages across the capacitors.

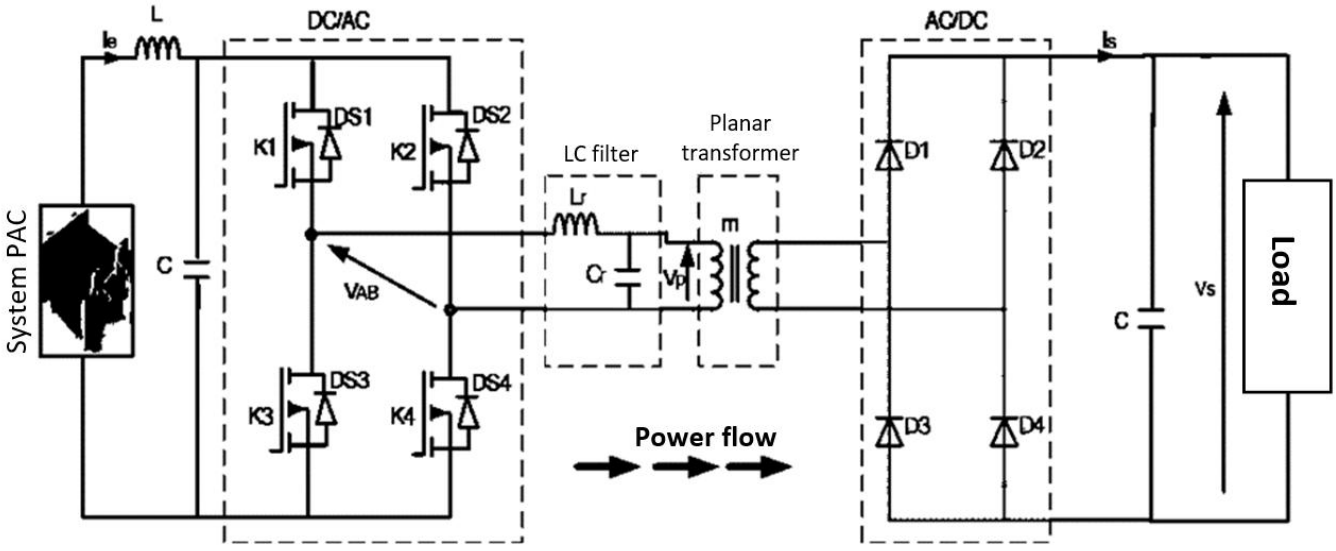

Fig. 4. Topology of the DC/DC converter on the PAC side [15], [16]

If all passive elements are linear, the differential equation describing a linear system is given by equation (7).

$$\dot{x}(t) = Ax(t) + Bu(t) \tag{7}$$

The system state vector is defined as the vector composed of the current flowing through the inductor (i_L) and the voltage across the capacitor (V_0). The control variable is the voltage supplied by the battery (VPAC) and the output variable is the DC bus voltage V_0.

$$\begin{cases} x = [i_L, v_0]^t \\ u = V_{PAC} \\ y = V_0 \end{cases} \tag{8}$$

The representation in the system state space is given by equation (9).

$$\begin{cases} \dot{x} = Ax + Bu \\ y = Cx + Du \end{cases} \tag{9}$$

If all impedances are reduced to the secondary windings, the equivalent diagram is shown in Figure 5 below [17].

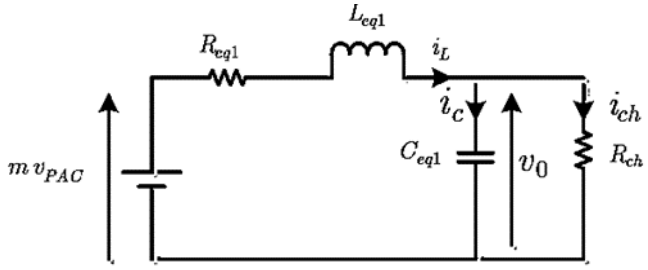

Fig. 5. The equivalent diagram of the converter

Where

$$\begin{cases} \dot{R_{eq1}} = 2r_0 + 2m^2 r_T \\ \dot{L_{eq1}} = L + m^2 L_r \\ \dot{C_{eq1}} = C_0 + \frac{C_r}{m^3} \end{cases} \tag{10}$$

Applying Kirchhoff's laws, we obtain:

$$\begin{cases} \frac{di_L}{dt} = -\frac{R_{eq1}}{L_{eq1}} i_L - \frac{1}{L_{eq1}} v_0 + \frac{m}{L_{eq1}} v_{PAC} \\ \frac{dv_0}{dt} = \frac{i_L(t)1}{C_{eq1}} - \frac{1}{R_{ch}C_{eq1}} v_0 \end{cases} \quad (11)$$

The matrix form of equation (11) is:

$$\begin{pmatrix} \frac{di_L}{dt} \\ \frac{dv_0}{dt} \end{pmatrix} = \begin{pmatrix} -\frac{R_{eq1}}{L_{eq1}} & -\frac{1}{L_{eq1}} \\ \frac{1}{C_{eq1}} & -\frac{1}{R_{ch}C_{eq1}} \end{pmatrix} \begin{pmatrix} i_L \\ v_0 \end{pmatrix} + \begin{pmatrix} \frac{m}{L_{eq1}} \\ 0 \end{pmatrix} . v_{PAC} \quad (12)$$

Therefore, the state model at time dT is:

$$\begin{cases} \dot{x} = Ax + Bu \\ y = Cx \end{cases} \quad (13)$$

With: $$\begin{cases} A = \begin{pmatrix} -\frac{R_{eq1}}{L_{eq1}} & -\frac{1}{L_{eq1}} \\ \frac{1}{C_{eq1}} & -\frac{1}{R_{ch}C_{eq1}} \end{pmatrix} \\ B = \begin{pmatrix} \frac{m}{L_{eq1}} \\ 0 \end{pmatrix} \\ C = (01) \end{cases} \quad (14)$$

2.2.5 Design Methodology For Interleaved Boost Dc/Dc Converters For Fuel Cell Electric Vehicles

In our application, we consider a 3-arm interleaved DC/DC boost converter to be the best converter in terms of input ripple reduction, according to reference [16]. The architecture of this type of converter is shown in Figure 6.

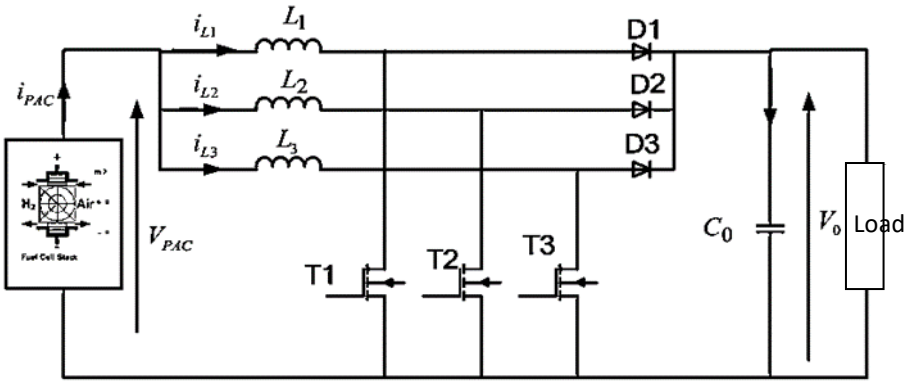

Fig. 6. Topology of a 3-phase interleaved BOOST DC/DC converter [16]

In order to determine the average model of this converter, four state variables were chosen: the voltage across the capacitor (V0) and the currents flowing through the inductors (iL1, iL2, and iL3). The state representation of the system is given by the following system of equations:

$$\begin{cases} \dot{x} = Ax + Bu \\ y = Cx \end{cases} \quad (15)$$

$$\begin{cases} \dot{X} = [i_{L1}, i_{L2}, i_{L3}, v_0]^t \\ U = [V_{PAC}, i_{ch}]^t \\ Y = V_0 \end{cases} \quad (16)$$

$$\begin{cases} \begin{pmatrix} \frac{di_{L1}}{dt} \\ \frac{di_{L2}}{dt} \\ \frac{di_{L3}}{dt} \\ \frac{dv_0}{dt} \end{pmatrix} = \begin{pmatrix} -\frac{(dr_\tau+(1-d).r_D}{L} & 0 & 0 & \frac{d-1}{L} \\ 0 & -\frac{(dr_\tau+(1-d).r_D}{L} & 0 & \frac{d-1}{L} \\ 0 & 0 & -\frac{(dr_\tau+(1-d).r_D}{L} & \frac{d-1}{L} \\ \frac{1-d}{C_0} & \frac{1-d}{C_0} & \frac{1-d}{C_0} & 0 \end{pmatrix} * \begin{pmatrix} i_{L1} \\ i_{L2} \\ i_{L3} \\ v_0 \end{pmatrix} + \begin{pmatrix} \frac{1}{l} & 0 \\ \frac{1}{l} & 0 \\ \frac{1}{l} & 0 \\ 0 & -\frac{1}{C_0} \end{pmatrix} * \begin{pmatrix} V_{PAC} \\ i_{ch} \end{pmatrix} \\ Y = (0 \quad 0 \quad 0 \quad 1) * \begin{pmatrix} i_{L1} \\ i_{L2} \\ i_{L3} \\ v_0 \end{pmatrix} \end{cases} \quad (17)$$

3 RESULTS AND DISCUSSION

3.1 EVALUATION CRITERIA

In order to conduct a proper comparative study, it was necessary to define the criteria for evaluating the converters. To this end, we opted for four key criteria:

- THD, which defines the level of network pollution resulting from harmonics (current, voltage); a network is considered unpolluted if its harmonic distortion is less than or equal to 5%;
- Power factor, which quantifies the amount of reactive energy absorbed;
- Efficiency, which allows us to evaluate the conversion rate; for a converter, the efficiency must be greater than or equal to 70%;
- Stability, which refers to the duration of the transient state.

3.1.1 HARMONIC DISTORTION RATIO

The harmonic distortion rate is shown in Figure 7.

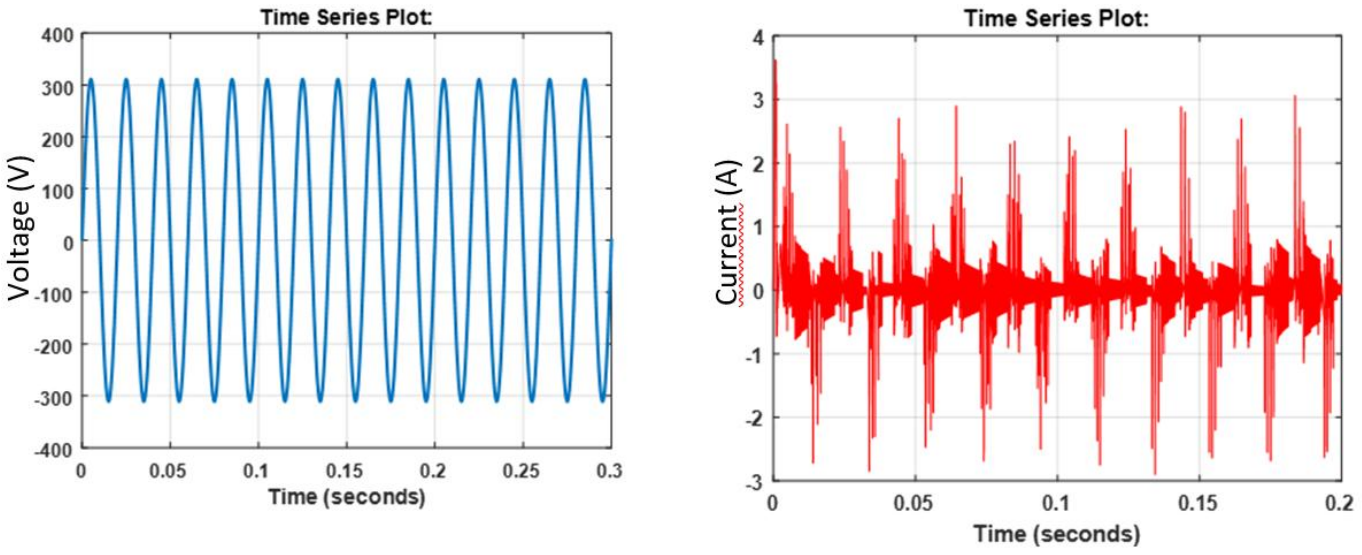

Fig. 7. Current and voltage curve on the AC side

We observe a highly disturbed current waveform, while the voltage waveform is perfectly sinusoidal. At first glance, this converter disturbs the grid and pollutes it with current harmonics.

Analysis of the THD will allow us to verify this assertion. The figure below shows the THD in voltage and current.

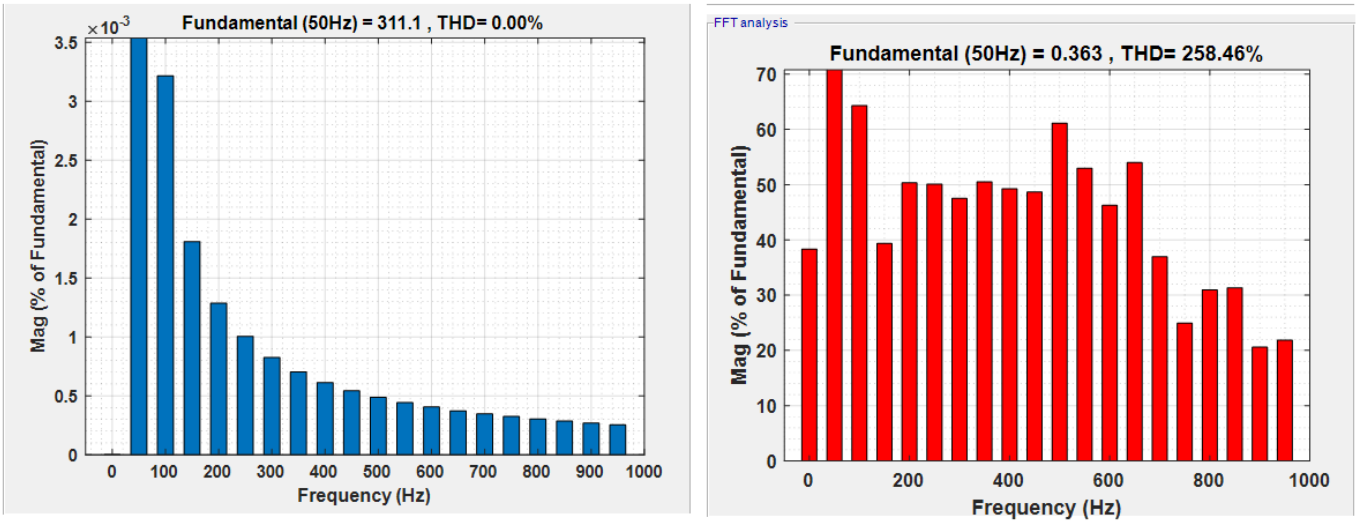

Fig. 8. Voltage and current THD

Analysis of these curves shows a highly abnormal current THD. This makes this converter highly polluting when the AC/DC side is connected to the grid in reversible mode.

3.1.2 POWER FACTOR

The power factor is simply the ratio between active power and apparent power, as shown in the formula below:

$$FP = \frac{P}{S} \tag{18}$$

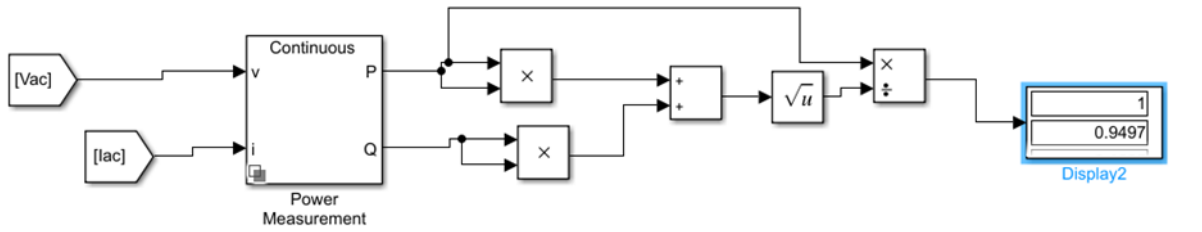

Fig. 9. Power factor measurement

The power factor in this converter is 0.9497, which is a fairly good value when compared to IEEE standards, which define a good PF as greater than or equal to 90%.

3.1.3 SYSTEM EFFICIENCY

Efficiency is the ratio between output power and input power; the closer the ratio is to unity (1), the better the efficiency. However, for a system not to operate at a loss, its efficiency must initially be at least 50%.

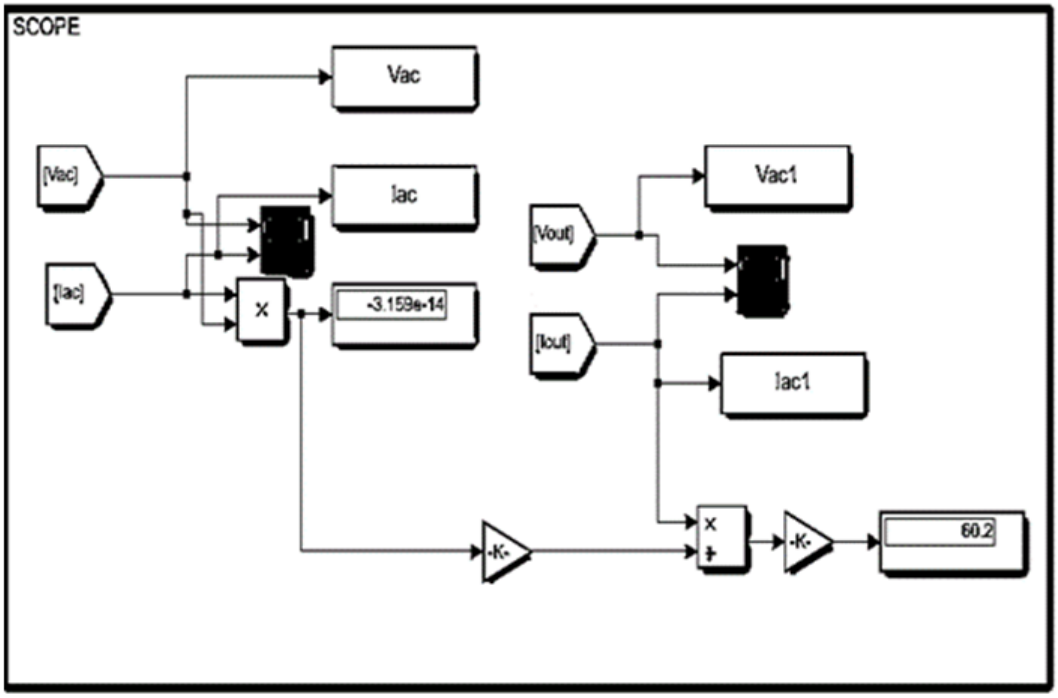

Fig. 10. AC/DC and DC/AC efficiency measurement

In this topology, the conversion rate is low at 60.2%.

3.1.4 System Stability And Speed

The stability of our system is shown in Figure 11.

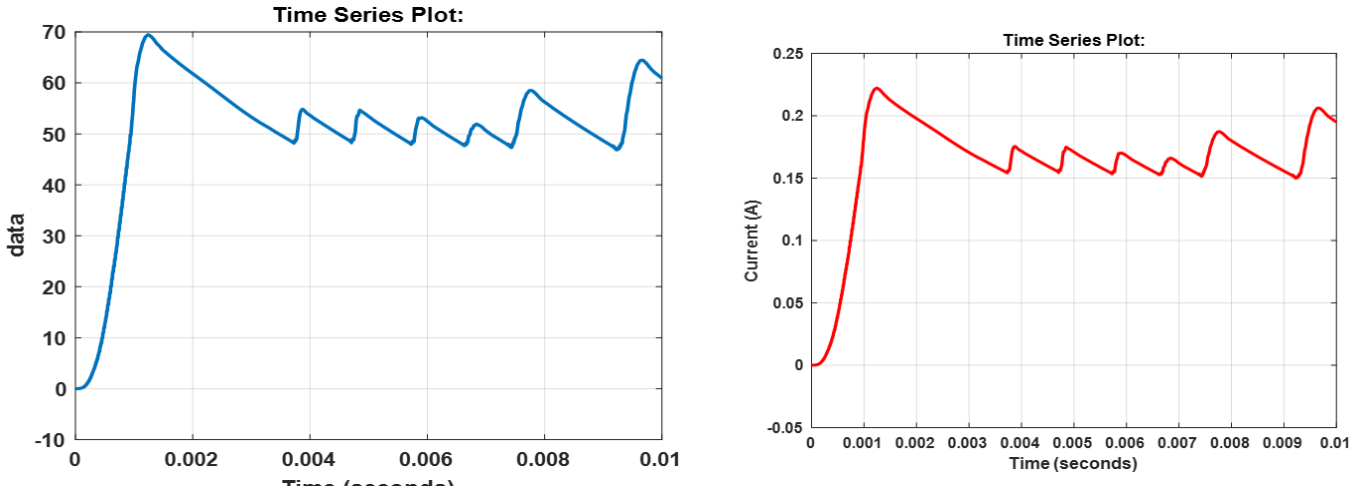

Fig. 11. System stability

The transient state lasts for 0.004 seconds. Our system is stable because the transient state lasts only a fraction of a second (4/1000 of a second).

3.2 Interpretation Of The Results Obtained

3.2.1 Total Harmonic Distortion (THD)

We observe a very stable current waveform, while the voltage waveform is perfectly sinusoidal. At first glance, this converter does not cause much disturbance.

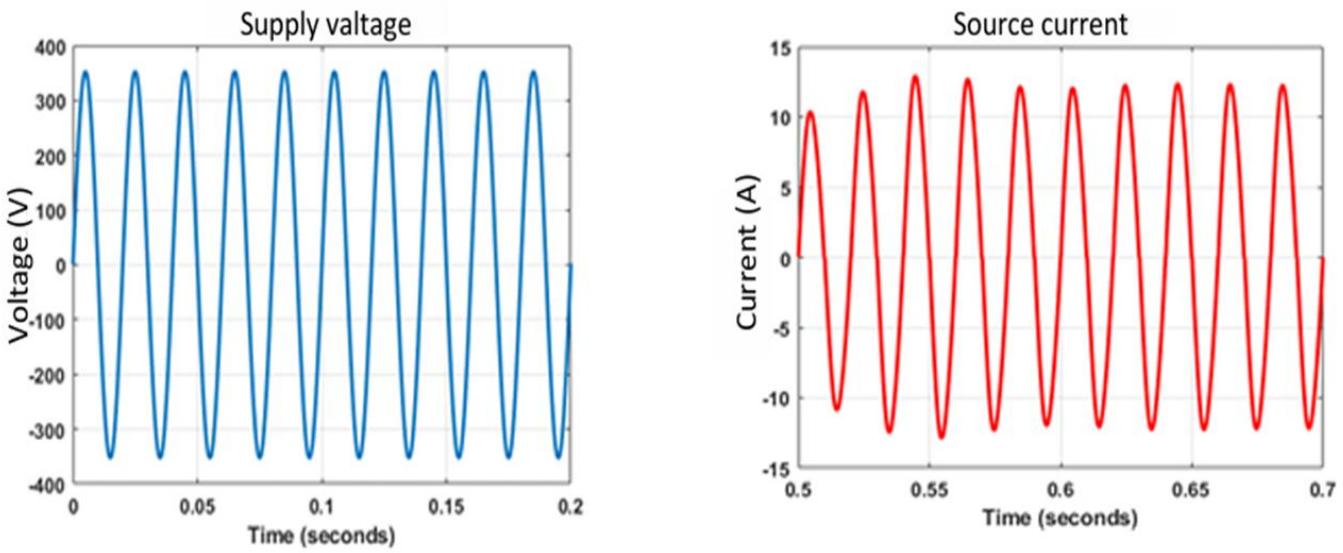

Fig. 12. Converter source voltage and current

Analysis of the THD will verify this assertion. The figure below shows the THD in voltage and current.

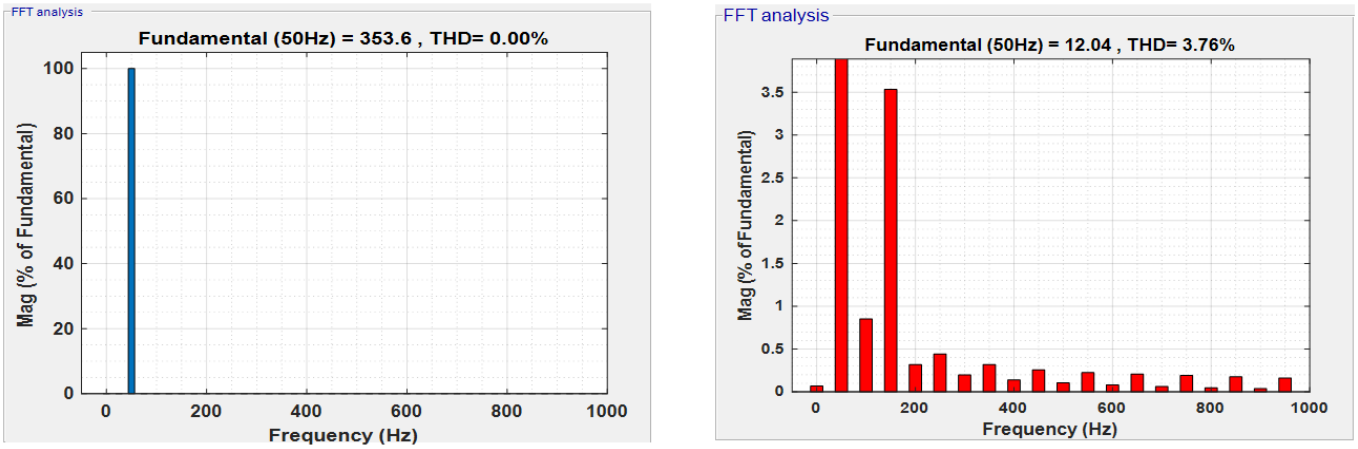

Fig. 13. Voltage and current THD

Analysis of these curves shows very good current THD. This makes this converter, from a network quality perspective, clean or non-polluting when connected to the AC/DC side of the network in reversible mode.

3.2.2 POWER FACTOR

We observe a very stable current waveform, while the voltage waveform is perfectly sinusoidal. At first glance, this converter does not cause much disturbance.

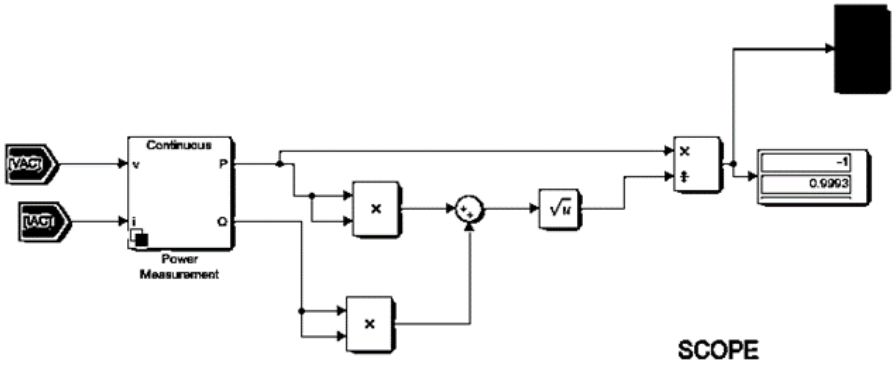

Fig. 14. Power factor measurement in the converter

3.2.3 EFFICIENCY

Efficiency is the ratio between output power and input power; the closer the ratio is to unity (1), the better the efficiency**.**

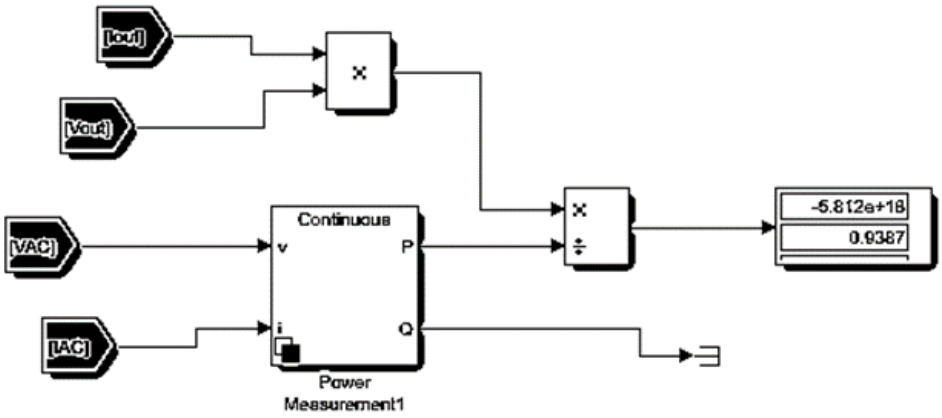

Fig. 15. Measuring the efficiency of the interleaved DC-DC boost converter

We can see that the conversion rate is very high in this converter topology (93.87%). This minimizes losses to around 7% in theory.

3.2.4 SYSTEM STABILITY AND SPEED

Speed is estimated by the time taken to reach the DC bus setpoint. Stability is the variation around the setpoint; if this variation is too significant, then the system is unstable.

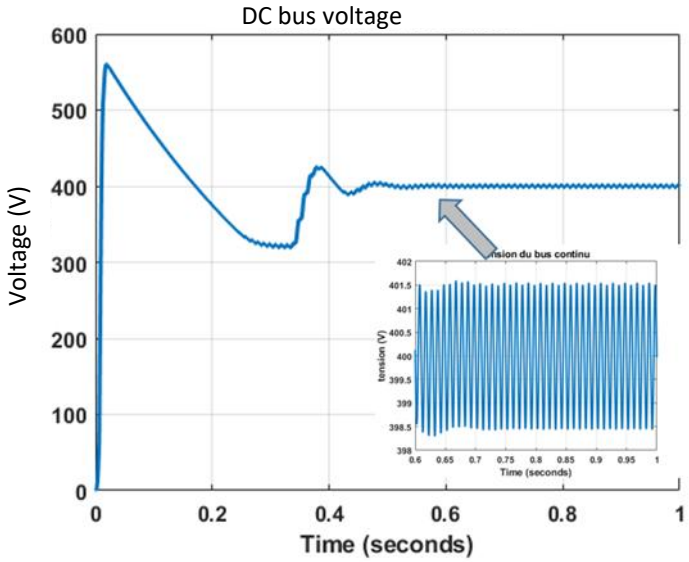

Fig. 16. DC bus voltage

The time taken by the DC bus to reach the setpoint value is 0.487 seconds. This is relatively slow. In conclusion, this converter is not fast when it comes to DC bus regulation.

Voltage variations around the setpoint are +/- 1.5 V, which is a significant value. Some articles define a standard of +/-10% of the setpoint for proper operation.

3.3 Performance Verification Based On Simulations

We can also see in Figure 17 (right) that ZVS mode is maintained throughout almost the entire transient. However, even though these transients would ultimately be damped in reality (here, the load variation is at 50Hz, which is very fast), this configuration is hardly acceptable.

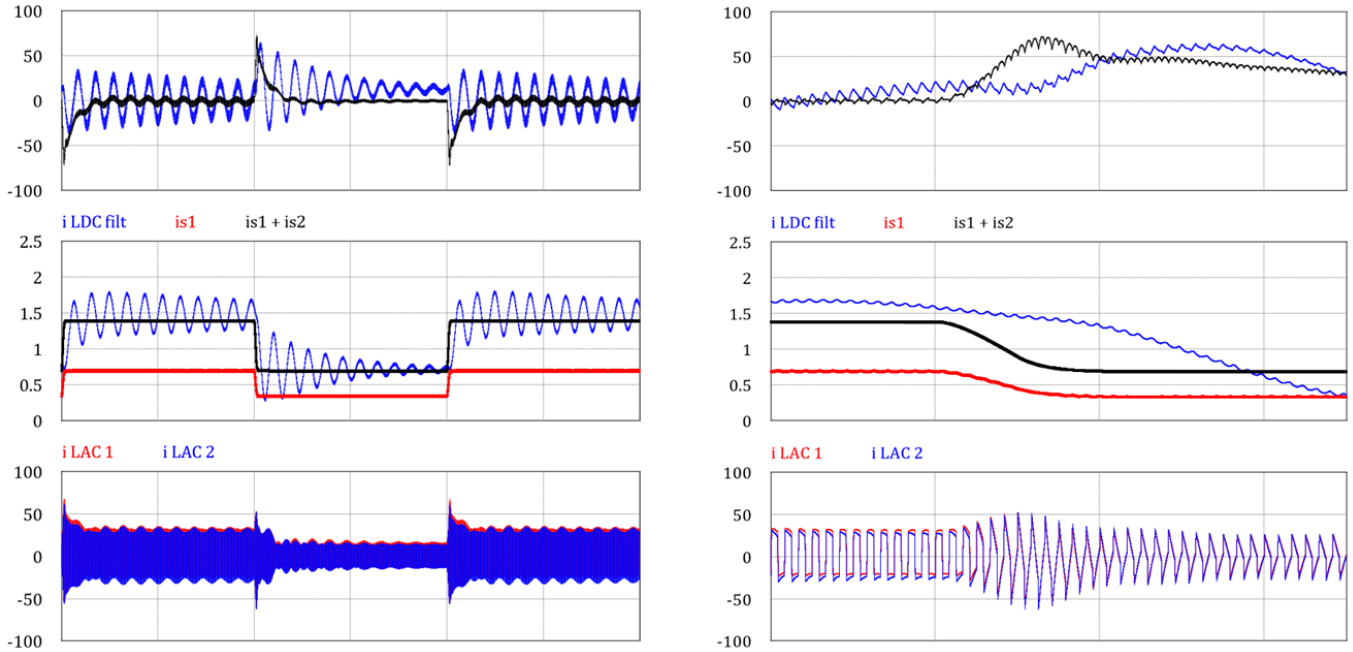

Fig. 17. Simulation results. Unregulated BOOST, voltage-regulated DAB

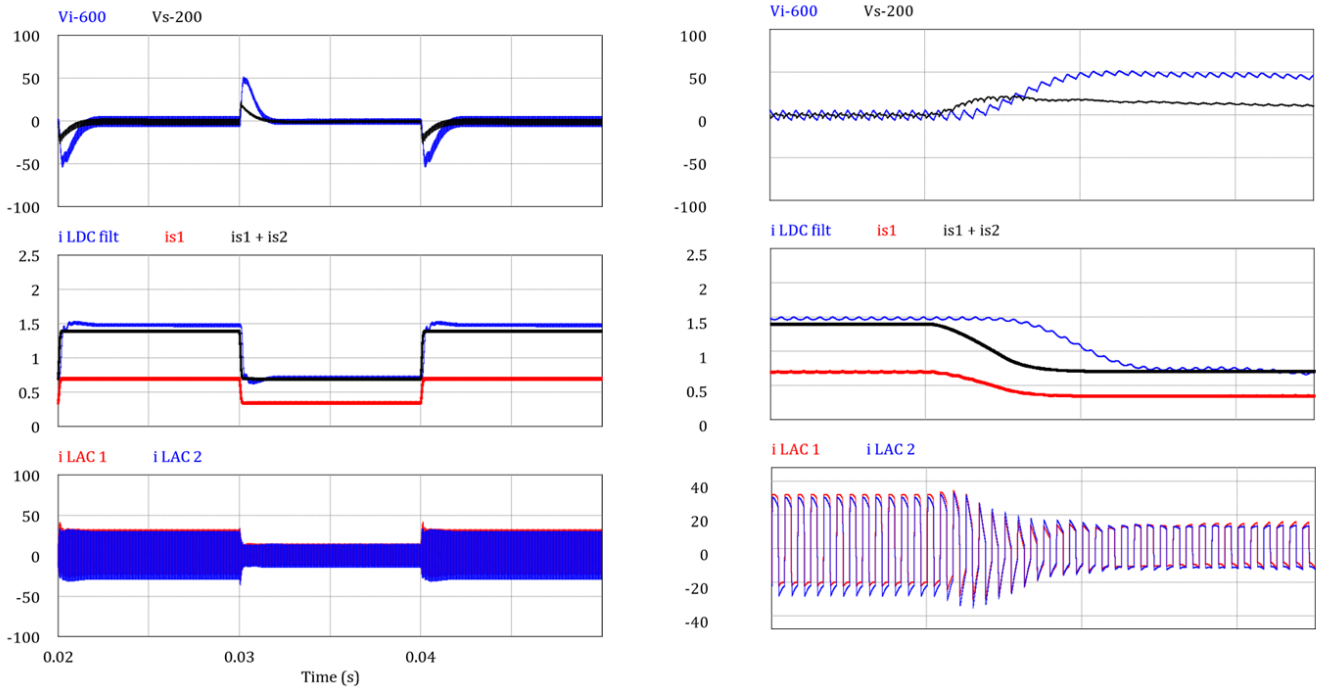

Fig. 18. Simulation results. Regulated BOOST, voltage-regulated DAB

Figure 18 shows the evolution of the same variables in the case where the BOOST is voltage regulated with an internal input current loop. As expected, the transient is controlled, particularly on the input current. The behavior of the DAB is virtually unchanged; the disturbances associated with the open-loop BOOST transient have simply disappeared.

These different results demonstrate that the principle of dual regulation without coupling between the two groups of loops, with the exception of proportional voltage setpoints, works and achieves very satisfactory performance, at least in theory. Nevertheless, it is well known that implementation problems can arise, particularly due to the inevitable noise fed back into the entire control chain by the switching. This system should be tested at ECA as an industrial extension of this work.

3.4 QUANTITATIVE COMPARISON OF THE DIFFERENT SOLUTIONS

In this section, we will compare the different final structures (with or without a pre-regulator stage) in terms of the critical aspect of losses in semiconductors. We will add a few qualitative comments on magnetic components, but it was extremely difficult to carry out a reasoned analysis on this aspect.

This exercise is very delicate because it requires the use of Spice models of components whose accuracy and scope of validity remain average. We have attempted to overcome these limitations through various experimental characterizations, but these cannot cover the entire spectrum of constraints encountered in the converters under consideration, in this context with widely variable input voltage. Furthermore, given these problems, it would be unrealistic to conduct such a comparison considering several component references. The first restriction we therefore imposed on this analysis was the choice of a single SiC MOSFET component, which we consider, at the time of writing, to be the most efficient of the various components we have had the opportunity to test (half a dozen). This is the C3M0016120K 1200V-16mΩ MOSFET, which has impressive combined conduction/switching characteristics. Even for the output side bridge under 200V, we have not found any competitors capable of rivaling it, as the 300-400V ranges are not very well developed for Si MOSFETs.

This situation provides a certain degree of comfort, as we find ourselves with a single component capable of operating effectively in all voltage ranges of our converter. Given our opinion on this component, we believe that what we have introduced as a restriction is not really one, since we will be comparing the different topologies based on the use of a component that should allow us to get the best out of each of them. Let us recall the main parameters of the loss model established for this component: The junction temperature value was arbitrarily set at 80°C, given that this parameter should not have a significant impact on the hierarchy of results. It should be noted that this model is based on data from datasheets and experimental measurements conducted in the 10-20A range. For higher current values, it is likely that the actual losses will be significantly higher than those given by this model, as the datasheets clearly show an increase greater than the order of 1 for currents between 30 and 60A.

Based on this choice, which greatly simplified our approach, we had to decide what we wanted to compare. Remaining faithful to our quest for the best performance and therefore to the principle of "one cell/two rather over-calibrated chips," we decided to "compete" with the same number of components/chips. We then converged on 10 cells (5 complete bridges) 20-35A for the 200V/15kW version and 8 cells (4 complete bridges) 20-35A for the 400V/15kW version, knowing that the cell voltage can reach 700-800V with the SiC MOSFET considered (Table 1). This implies that in ZVS-PSFB and SRC structures, the rectifiers are synchronous, i.e., made with MOSFETs assumed to be synchronized with the operation of a diode bridge.

We have selected the following configurations to build a 15kW half converter:

Table 1. Options selected for a 15kW half converter

Solution				**VV_{DD}=220000V VV_{DD}=990000V**
Floor 1	DAB VV_{DD}=220000V VV_{DD}=990000V m = 0.4 m = 0.8 L_{AC} = 13.8µH		Optimized sizing for: Number of primary bridges and Number of secondary bridges:	VE ref = 500V in parallel
	ZVS-P VV_{DD}=220000V L_S = 47.1µH m = 1.11	SFB VV_{DD}=990000V L_S =188.6µH m = 2.22	Optimized sizing for:	VE = VE MIN = 200V
			Number of primary bridges:	1 in parallel
			Number of secondary bridges:	2 in series
	SRC		Optimized sizing for:	VE = VE MIN = 200V
	VV_{DD}=220000V VV_{DD}=990000V		Number of primary bridges:	2 in parallel
	m = 1 m = 2 L_R = 22.5µH C_R = 312.5nF		Number of secondary bridges:	3 in parallel
Floor 2	BOOST + DAB VV_{DD}=220000V VV_{DD}=990000V m = 0.333 m = 0.667		Optimized ATM sizing for:	V_i = 650V
			Number of BOOST bridges:	2 in parallel
			Number of primary DAB bridges:	1 in series
	L_{AC} = 20µH L_{DC} = 280µH		Number of secondary DAB bridges:	2 in parallel

An important piece of information is the effective current level in the cells in each case at the critical input voltage of 200V. The table below summarizes the situation. As already indicated above, it is immediately apparent that the secondary side of the DAB is extremely constrained.

Table 2. Effective currents of semiconductor components for minimum input voltage VE = 200V

Solution			**V_E = 200V**	**VV_{DD}=220000V VV_{DD}=990000VV**
Floor 1	DAB		ITiE eff ITiS eff	31.8A 55RR.00A 39.7A
	ZVS-PSFB		ITiE eff ITiS eff	29.46A 17.7A 26.5A
	SRC		ITiE eff ITiS eff	29.45A 19.6A 14.7A
Floor 2	BOOST + DAB	BOOST DAB	ITiE eff ITiS eff ITiE eff ITiS eff	16.6A 11.2A 19.2A 28.8A

The next step is to decide on the value of the switching frequency at which this comparison will be made. This is always a challenge in converter design, as defining an optimal value would require reliable, "broadband" representation models for all components in order to then apply an optimization procedure. This approach is virtually impossible for AC-HF magnetic components, as there are no fixed technological structures and estimating losses remains very difficult (strong interdependence between geometry and losses). We are therefore forced to make a choice that is highly arbitrary and relies heavily on experience.

4 CONCLUSION

With increasing constraints on energy resources and environmental concerns, electric vehicles will attract more interest from the automotive industry and consumers. Although their market share is still insignificant today, it can be predicted that electric vehicles will gradually gain popularity in the market due to fuel savings and superior vehicle performance. Modeling and simulation will play an important role in the successful design and development of this type of vehicle. At the end of this research, two original power converter structures for fuel cell electric vehicles were proposed and explored. The role of this converter is to condition the voltage and current levels and waveforms from the source (fuel cell) to those of the vehicle's DC bus, to which the inverter supplying the vehicle's traction motor is connected. A bibliographic study was conducted. This study enabled us to examine the hybrid and electric vehicles available on the market, primarily fuel cell and supercapacitor vehicles. We presented the energy chain structure of this type of vehicle. We showed that the choice of power converters used depends on several criteria, such as efficiency, energy density, and response time. We also presented the different existing topologies of isolated and non-isolated DC-DC converters, along with their advantages and disadvantages. Consequently, a DC-DC converter is essential to increase the voltage level to that of the DC bus. The isolated parallel resonance DC-DC converter and the non-isolated interleaved DC-DC converter meet the requirements for electric vehicle applications. We analyzed and sized these two DC-DC converters. A dynamic model was developed and verified by simulation in the Matlab/Simulink environment with different driving conditions used for a standard speed cycle.

REFERENCES

[1] J Hofstetter, P Boucharel, F Atzler... «Fuel consumption and emission reduction for hybrid electric vehicles with electrically heated catalyst», SAE International Journal..., 2020 - sae.org

[2] A.P.K. Yadav, S. Thirumaliah and G. Haritha, «Comparison of MPPT Algorithms for DC-DC Converters Based PV Systems», International Journal of Advanced Research in Electrical, Electronics and Instrumentation Engineering, Vol. 1, N°1, 2012.

[3] U. S. OTAM and B. L. Moffo, «Comparative study between duty cycle modulation and gigma-delta (ΣΔ) modulation based on analog to digital conversion», Journal of Electrical and Electronic Engineering, Vol. 16, No. 1, 2023, pp. 27-32.

[4] N.Ali, M.H. Tarafdar, B.B. Mohammad and Saeed Danyali, « A nonisolated multiinput multioutput DC–DC boost converter for electric vehicle applications | IEEE Journals & Magazine | IEEE Xplore ». https://ieeexplore.ieee.org/abstract /document/6823178/ (accessed on August 2, 2025).

[5] S. Farajdadian et S. M. H. Hosseini, « Optimization of fuzzy-based MPPT controller via metaheuristic techniques for stand-alone PV systems», Int. J. Hydrog. Energy, vol. 44, no 47, p. 25457-25472, oct. 2019.

[6] A.-F. Garçon, « La voiture électrique dans La Nature (1890-1900), approche micro-historique d'un échec technique«, Cahiers François Viète, no I-5, p. 17-43, 2003.

[7] B. G. Jeannot, M. J. Jacques, and M. M. Jeannot, « Reliability of the MPPT Control on the Energy Parameters of a Photovoltaic Generator», World J. Eng. Technol., vol. 8, no 3, Art. no 3, juill. 2020, doi: 10.4236/wjet.2020.83038.

[8] Afshan Ilyas, M. Rizwan Khan, Mohammad Ayyub, «FPGA based real-time implementation of fuzzy logic controller for maximum power point tracking of solar photovoltaic system», Optik - International Journal for Light and Electron Optics 213 (2020) 164668.

[9] Jyotheeswara Reddy K., Sudhakar N« Energy sources and multi-input DC-DC converters used in hybrid electric vehicle applications – A review - ScienceDirect ». https://www.sciencedirect.com/science/article/abs/pii/S0360319918322304 (accessed on September 2, 2025).

[10] S. Messalti, «Analysis of the transient stability of high-voltage direct current transmission networks (HVDC-FACTS)«, Thesis, 2018. [Online]. Available at: http://dspace.univ-setif.dz: 8888/jspui/handle/123456789/2253.

[11] M. Dhananjaya, D. Ponuru, T. S. Babu, B. Aljafari, and H. H. Alhelou, « A New Multi-Output DC-DC Converter for Electric Vehicle Application«, IEEE Access, vol. 10, p. 19072-19082, 2022, doi: 10.1109/ACCESS.2022. 3151128.

[12] K. Jyotheeswara Reddy et S. Natarajan, « Energy sources and multi-input DC-DC converters used in hybrid electric vehicle applications – A review », Int. J. Hydrog. Energy, vol. 43, no 36, p. 17387-17408, sept. 2018, doi: 10.1016/j.ijhydene.2018.07.076.

[13] A. de O. Ferreira, A. U. Brito, M. A. B. Galhardo, L. Ferreira, and W. N. Macêdo, « Modeling, control and simulation of a small photovoltaic-wind water pumping system without battery bank», Comput. Electr. Eng., vol. 84, p. 106619, juin 2020, doi: 10.1016/j.compeleceng.2020.106619.

[14] Souleman Njoya M. and O. Tremblay« A generic fuel cell model for the simulation of Fuel Cell Power Systems | IEEE Conference Publication | IEEE Xplore ». https://ieeexplore.ieee.org/abstract/document/5275853/ (accessed on August 2, 2025).

[15] B. Dich and N. Cherigui, «Study of a DC motor control system», Thesis, Ms. S. BOURI, 2020. [Online]. Available at: http://thesis.essa-tlemcen.dz: 8080/xmlui/handle/STDB_UNAM/77.

[16] S. Messalti, «Analysis of the transient stability of high-voltage direct current transmission networks (HVDC-FACTS)«, Thesis, 2018. [Online]. Available at: http://dspace.univ-setif.dz: 8888/jspui/handle/123456789/2253.

[17] F.A. Mohammad, S.R. Siti Rohani, A.R. Nasrudin and N.A. Mohammad and A.B. Elmi, « Recent Developments in DC-DC Converter Topologies for Light Electric Vehicle Charging: A Critical Review ». https://www.mdpi.com/2076-3417/13/3/1676 (accessed on August 1, 2025).